Tribology: Surface Interaction Experiments

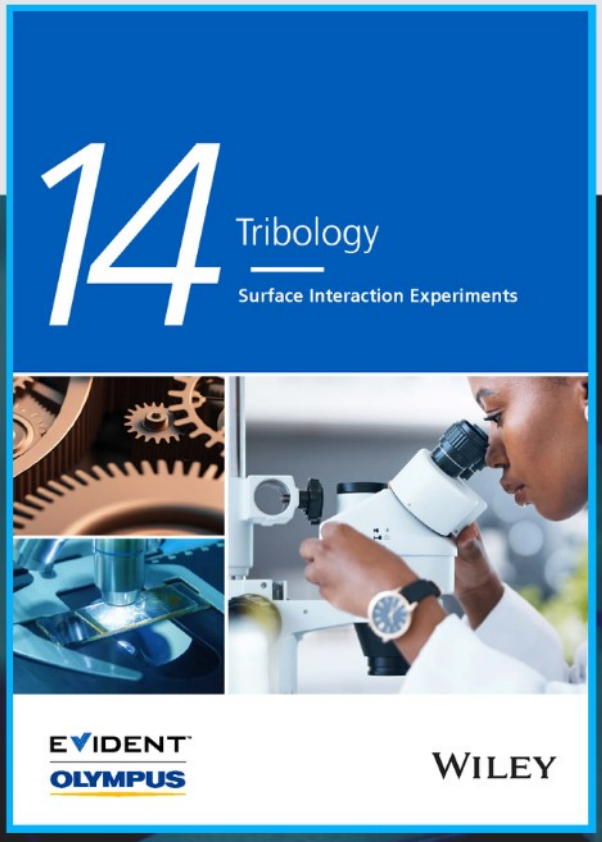

The latest eBook from Advanced Optical Metrology. Download for free.

Tribology has been a critical part of human civilization since ancient times, and it continues to play a crucial role in modern industries. Evident's eBook, in collaboration with Wiley, covers a broad range of topics, including the wear, friction, and lubrication of surfaces, testing methods, and the latest research on tribological phenomena at the nanoscopic level.

Don't miss out on the opportunity to dive into the world of tribology and gain a better understanding of the interaction of moving surfaces. Download our eBook now and stay ahead in the field of tribology.

EVIDENT
OLYMPUS

WILEY

Received: 18 April 2022 | Revised: 23 August 2022 | Accepted: 23 August 2022

DOI: 10.1002/pen.26130

RESEARCH ARTICLE

POLYMER ENGINEERING AND SCIENCE WILEY

Oxygen transmission rate through thermoformed trays: Modeling and influence of processing variables

Carlos Enguix[1] | **Neus Sanjuan**[2] | **Javier Ribal**[3]

[1]AINIA, International Markets, Paterna, Valencia, Spain

[2]Department of Food Technology, Universitat Politècnica de València, Valencia, Spain

[3]Department of Economics and Social Sciences, Universitat Politècnica de València, Valencia, Spain

Correspondence
Carlos Enguix, AINIA, C/Benjamín Franklin 5-11, Parque Tecnológico de Valencia, E46980 Paterna, Valencia, Spain.
Email: cenguix@ainia.es

Abstract

The oxygen transmission rate (OTR) is a key parameter when selecting a sheet to make a thermoformed tray, as it influences the shelf life of packaged food. The OTR of a thermoformed tray depends on the distribution of the material's thickness over its walls. The goal of this study is to model the evolution of oxygen in the headspace of a thermoformed plastic tray considering the thickness distribution of its walls. PET/PE films with different thicknesses and a PET/PE/EVOH/PE structure with EVOH acting as a barrier layer were used for the thermoformed trays. The thickness of the thermoformed trays was measured at different points to determine the average thickness of the tray subsections. A model was built to predict the variation in the oxygen content inside the headspace over time. The results of the model were correlated with experimental data by regression analysis. The model can be used to perform a straightforward comparison of both different structures as well as the effect of the thickness of the layers that constitute the multilayer sheet. The model can also support decisions about the best multilayer for a particular tray design so as to achieve a specific product shelf-life.

KEYWORDS

barrier, diffusion, gas permeation, modeling, polyesters

1 | INTRODUCTION

Plastic thermoforming and plastic injection are both commonly used to manufacture packaging trays, although thermoforming is more widespread for economic reasons. In addition, thermoforming allows multilayer sheets to be used, which provides a barrier to gases so as to achieve the required product shelf-life in the case of using a modified atmosphere.[1]

Multilayer sheets are composed of different materials with different functions, namely sealing, structure (mechanical behavior against loads), and barrier. The final features of a thermoformed tray, such as the gas transmission rate or mechanical properties, depend on the material used, the geometry of the tray, and its thickness distribution.[2] During the thermoforming process, the sheet is heated and stretched against a mold by applying vacuum and pressure, and consequently, the thickness of the tray changes from one point to another; the most stretched parts of the initial sheet, especially the base corners, are those that are the least thick. The stretching generates changes in the ordering of the

polymer chains, mainly reorientation, restriction of chain mobility, and recrystallization,[3,4] generating changes in the above-mentioned features.[5] Hence, care must be taken to ensure that, after thermoforming, the barrier layer remains thick enough along the formed container to preserve the gas barrier properties. This is the case of multilayers, such as PP/EVOH/PP, A-PET/PE/EVOH/PE or PA/EVOH/PA/PE.

The shelf-life of a packaged food depends, among other features, on the oxygen permeating the package. In many cases, the oxygen enters the packaging, accelerating oxidation reactions and microbiological growth, although, in high concentrated oxygen atmospheres, such as packaged raw beef, permeation takes place from the inside to the outside. The oxygen transmission rate (OTR) is the amount of oxygen transferred per unit of time through a surface of packaging material.[6] The final oxygen concentration in a package at a specific period after filling and closing will depend, on the one hand, on the initial oxygen content[7,8] and, on the other hand, on the quantity of oxygen that flows throughout the walls of the package. The changes in the oxygen concentration can be calculated as the integration of the OTR through the package surface during a specific time, the OTR being a consequence of the permeability of the materials, the thickness distribution after thermoforming, as well as it is proportional to the driving force, originated by the difference of partial pressure or concentration of a permeant inside and outside the package.[9] Exceptions to this occur for other permeants that interact with the packaging material, which is the case of organic permeants such as some flavor and aroma compounds. The permeability of a packaging material is a product of the diffusivity and solubility coefficients, the latter determined by the polymer-permeant interaction, free volume and temperature. For polymers forming crystalline regions, such as PET, Zekriardehani et al.[10] described a simple two-phase transport model based on the impermeability of a crystal phase dispersed in a permeable amorphous matrix.

Non-uniform wall thickness distribution is affected by processing parameters, such as mold temperature, film or sheet temperature, or processing time. These parameters are closely related to the thermoforming window, that is, the range of thermoforming temperatures of the polymers used.[11,12] Furthermore, thermoforming optimization is even more complicated when processing a multilayer structure with different polymers. OTR is often quoted as a specification in the technical sheet of the multilayer material. However, the OTR of a thermoformed material cannot be easily extrapolated from the OTR of the original sheet material[13,14] and it must be estimated since it allows the evolution of oxygen content inside the package to be modeled in order to determine the product shelf-life. Peterson et al.[14] predicted the OTR of final thermoformed packages based on the OTR of the unconverted sheet and the area of the tray after thermoforming by measuring the thickness at different points and assessing whether the thickness measurements are suitable for estimating the OTR. These authors concluded that it is not possible to present an equation to estimate the OTR that is suitable for any polymer combination.[14]

The food industry is interested in estimating the OTR of a package from the permeability data of the unconverted sheet, instead of measuring the OTR of the resulting package.[5,14] Hence, the goal of this study is to model the evolution of oxygen in the headspace of a thermoformed plastic tray considering the thickness distribution of its walls. To this end, trays of different multilayer materials have been thermoformed and the thickness distribution has been measured to estimate the OTR of each package and to model the oxygen entry in the packages over time. In this way, the evolution of the modeled oxygen content has been compared with the experimental measurements, and the correlation between the real entry of oxygen into the package and the modeled has been determined. In addition, the subsections of the tray that contribute the most to the oxygen concentration inside the tray have been identified.

2 | EXPERIMENTAL

2.1 | Sheets and film for the lid

Thermoformed trays were made with different commonly used multilayer sheets, specifically, sheets of 450, 550, 600, and 650 μm A-PET/PE with 40 μm of PE (Klöckner Pentaplast, Spain), and a sheet of 750 μm A-PET/PE/EVOH/PE with approximately 20 μm EVOH and two layers of 40 μm PE (Klöckner Pentaplast, Spain). For the lid, an OPET/PE/EVOH/PE multilayer with 8 μm of EVOH was selected due to its high oxygen barrier capacity. In this way, the oxygen permeation in the closed containers was mostly due to the most stretched subsections of the tray.

2.2 | Tray thermoforming

A Multivac R230 (Multivac, Germany) thermoforming machine was used. The machine is equipped with: (a) two heating plates; (b) one forming unit to make up the preheated sheet inside the mold using vacuum and compressed air; (c) one sealing unit that, before sealing, removes the air inside the tray and allows a combination of gases to be introduced to obtain a modified atmosphere.

For each sheet, process parameters were selected after previously performing some tests to check that the

TABLE 1 Main thermoforming parameters applied to each sheet

	Sheet thickness (μm)				
	450	**550**	**600**	**650**	**750**
Heating time (s)	2.5	3	3.5	3.75	4.2
Pressing time (s)	0.02	0.02	0.02	0.02	0.5
Forming time (s)	3	3.5	3.5	3.5	3.5
Forming pressure (bar)	1.5	1.5	1.5	1.5	2
Security time (s)	1	1	1	1	0.5

material adapts to the surface of the mold, preventing transparency changes that could happen if the sheet is overheated, which could recrystallize the molecules. It must be borne in mind that the heating of semi-crystalline polymers, such as PET, is characterized by the transformation of the state of the sheet from glassy into rubbery. The temperature at which this transition occurs is named the glass transition temperature (Tg), and the temperature range for which the polymer is sufficiently flexible to be stretched and formed is called the forming window.[15]

A specific *heating time* is needed to heat the sheet until it reaches an optimal thermoforming. Throughout the heating time, the sheet lies between the two heating plates but without touching them. The *pressing time* is the time during which the heating plates are in contact with the sheet, and the *forming time* is the time needed to thermoform the sheet. During the forming time, the machine presses on the sheet to fit into the mold and then it applies pressure to form the tray. At the same time, the machine extracts the air from the surface of the mold (which has small holes to produce the suction of the sheet). When the sheet is in contact with the cold mold (which has a refrigerated system), its temperature falls and when the plastic material is cold enough to keep the shape of the mold, the tray is extracted from it. To this end, a *security time* is established, which is the time added to the forming time prior to extracting the tray from the mold.

For the PET/PE sheets (450, 550, 600, and 650 μm), the heating temperatures used in the thermoforming process were 95°C, 100°C, 105°C, and 110°C, whereas for the PET/PE/EVOH/PE sheet (750 μm) the heating temperatures were 105°C, 110°C, 115°C, and 120°C. Table 1 shows the time of the processing steps and the forming pressure parameters. As expected, the thicker the sheet, the longer the time needed to reach a uniform temperature throughout the sheet. For each case study (combination of material–thickness–temperature), 30 units were made, with a total of 600 trays (5 sheets × 4 temperatures × 30 repetitions). Then, the air inside the trays was replaced by nitrogen to reach a residual oxygen content close to 0.01 atm partial pressure and the lid was sealed.

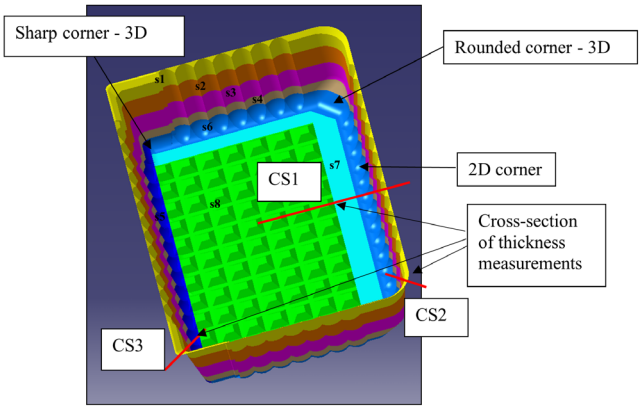

FIGURE 1 Subsections considered in the thermoformed tray

2.3 | Thickness measurement

A handheld thickness gauge (Magna Mike 8500, Olympus, Tokyo, Japan) was used to determine the thickness distribution of the trays.

The tray design has four 3D corners, of which two are sharp corners and the other two are rounded (Figure 1). According to previous experiments, the thickness was measured at 20 points of each tray (Figure 2) as the average of the 30 measurements corresponding to each manufactured unit. The gauge utilizes a magnetic method to make reliable and repeatable measurements on nonferrous materials. Measurements were made by holding the probe on the selected points of the external side of the trays and placing a small steel target ball of diameter 1.59 mm inside of the trays, with an accuracy of ±3%, and a resolution of 0.001 mm. A Hall-effect sensor placed in the probe measures the distance between the probe tip and the target ball.

2.4 | Measurement of oxygen content evolution

The evolution of the oxygen content inside the tray was measured with Fibox 3 (PreSens Precision Sensing GmbH, Germany), a fiber-optic device for precise oxygen concentration measurements. PSt3 oxygen sensors (detection limit 15 ppb, 0%–100% oxygen) were placed inside the trays after thermoforming and before sealing. As temperature influences the OTR of the trays, once sealed, the trays were stored in a temperature-controlled chamber at 20°C. It must be noted that Fibox 3 trace is temperature compensated; therefore, precise measurements can be taken without being affected by potential changes in the

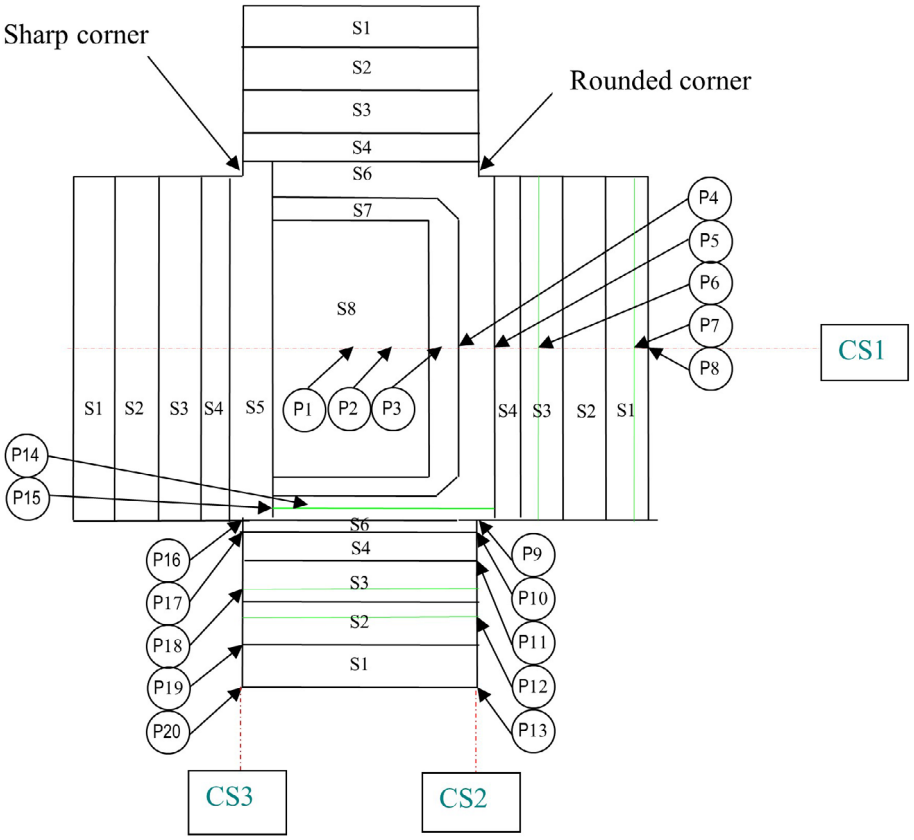

FIGURE 2 Subsections (s_1 to s_8), cross sections (CS), and points of the thermoformed tray where the thickness was measured

temperature. The oxygen content was measured for 150 days at 20°C, namely every 5 days during the first 30 days, and every 30 days during the following 120 days.

2.5 | Permeability

The permeability of each sheet has been obtained from the technical fact sheets and contrasted against experimental measurements by using Mocon Ox-Tran 2/21 (Minneapolis, MN, USA), at 23°C and 0% relative humidity, according to the ASTM F1927 standard.[16]

2.6 | Estimation of thickness and surface area

Eight subsections were defined to model the evolution of the oxygen content inside the package (Figures 1 and 2). Four of these subsections (s_1 to s_4) correspond to the lateral strips, and were divided into four rectangles, each one corresponding to a wall of the tray. Subsections s_5 to s_8 are located at the bottom of the tray. The surface area of the subsections was calculated with the Catia v5 software for CAD/CAE.

The average thickness (d_i) of each subsection (s_i) was calculated from the thickness measured at the 20 points of the trays. The average thickness of the respective vertices has been considered for the purposes of calculating the average thickness of the rectangles of the lateral strips. In the event that the thickness of a vertex was not measured, it was extrapolated from the thickness of the adjacent points in the same section. The average thickness of each subsection, s_1 to s_4 and s_6, was calculated as the weighted average of the four rectangles into which the subsection is divided, considering the surface area of each rectangle for ponderation purposes. The thickness of s_5 corresponds to that of P15, whereas for s_7 the average thickness of points P3 and P14 was calculated. As to s_8, the average thickness of P1 and P2 corresponds to that of the central part of the subsection and the average of P14, P3, and P15 has been taken for the sides. Then, the thickness of s_8 has been calculated as the weighted average of the thickness of the central part and the sides.

2.7 | Modeling oxygen permeation through the tray walls

For each time interval, the model integrates the OTR of each subsection of the tray, including the lid, and predicts the oxygen concentration in the headspace of the

tray after a specific time. For this purpose, it was considered that the oxygen transmission rate of the tray (OTR_{tray}) is made up of the contribution of each layer m comprising the subsection (OTR_i). In turn, OTR_i is proportional to the area of the subsection ($A(s_i)$) and inversely related to the average thickness of the layer of the subsection (d_i), as given by Equation (1)[5]:

$$OTR_{tray} = \sum_{i=1}^{8} OTR_i = \sum \frac{A(s_i) \cdot d_0}{d_i} \cdot OTR_0, \quad (1)$$

where OTR_0 and d_0 are the OTR and the thickness of the unconverted sheet; d_i is the thickness of each subsection of the tray after thermoforming; and OTR_i is the OTR of each subsection.

In addition, the permeability of a gas through a packaging material can be expressed as[17]:

$$P = \frac{Q \cdot d}{A \cdot t \cdot \Delta P}, \quad (2)$$

where P is the permeability coefficient (cm^3 O_2·μm/m^2·day·atm); Q (cm^3) is the amount of permeant diffusing through a polymer of surface area A (m^2) over a period of time t (day); d (μm) is the wall thickness; and ΔP is the change in the partial pressure of the permeate across the film or sheet (atm).

From Equation (2) and taking into account that the transfer of molecules through the multilayer walls of the tray occurs by a sorption–diffusion–desorption mechanism, driven by the difference in partial pressure across the material, OTR_i can be calculated for each subsection as:

$$OTR_i = \frac{dn_t}{dt} = P \cdot (n_{ext} - n_t) \frac{A(s_i) \cdot R \cdot T}{d_i \cdot V}, \quad (3)$$

where n_t is the molar concentration of O_2 inside the tray (moles of O_2/cm^3) at time t (day); n_{ext} is the molar concentration of O_2 in the environment surrounding the tray; P is the permeability coefficient of the tray walls (cm^3 O_2·μm/m^2·day·atm); R is the gas constant (8.314 J/mol·K or 0.082 atm·L/mol·K); T is the temperature of the environment surrounding the tray (°K); and V is the headspace volume inside the tray (cm^3). As the tray is made of a multilayer structure with m layers, P/d_i may be calculated by using Equation (4)[17–19]:

$$P/d_i = \frac{1}{\frac{d_{i1}}{P_1} + \frac{d_{i2}}{P_2} + \ldots + \frac{d_{im}}{P_m}}, \quad (4)$$

where d_i is the average thickness of the tray subsection after thermoforming; d_{im} is the thickness of each layer m in this subsection; and P_m is the corresponding permeability of the layer m.

TABLE 2 Activation energy for oxygen permeation of the packaging materials used in the study[17]

Packaging materials	E_p (kJ/mol)
LDPE	42.700
EVOH 32	65.23
A-PET	37.70

For the calculations, the total storage time was divided into 50 intervals, which were used to calculate n_t and to plot the evolution of the oxygen content over time.

From the average thickness of each subsection (d_i), the theoretical thickness of each layer m (m corresponds to A-PET, PE, or EVOH, depending on the multilayer sheet) after thermoforming (d_{im}) was calculated by assuming that all the layers are reduced proportionally to the total thickness of the subsection.[5] Hence, the proportion d_i/d_0 is kept for all the layers, and $d_{im} = d_m \cdot d_i/d_0$; and it is thus possible to estimate the final thickness of each layer after thermoforming from the total thickness before and after thermoforming.

Additionally, the temperature effect on the permeability of each layer material P_m was determined by applying the Arrhenius equation[19]:

$$P_m = P_{m\_ref} \cdot \exp\left[\frac{E_p}{R}\left(\frac{1}{T_{ref}} - \frac{1}{T}\right)\right], \quad (5)$$

where P_m is the permeability of the polymer material at a specific temperature T (293 K in this study); P_{m_ref} (cm^3·μm/m^2·day·atm) is the reference permeability coefficient measured at T_{ref} (296 K); and E_p (kJ/mol) the activation energy of the permeability process. The values of E_p for the materials of each layer are shown in Table 2.

3 | RESULTS AND DISCUSSION

3.1 | Analysis of thickness distribution

The box-plots in Figure 3 show the thickness distribution for each thermoformed tray under the specified conditions as a result of 30 measurements at each point. In angle corner, taking into account that the thickness of each point is related to the material stretching during thermoforming, it can be observed that points P15, P16, and P17 are critical, achieving a thickness reduction of almost 90% with respect to the original thickness of the coextruded sheet. On the other hand, points P8, P13, and P20, which are close to the rim of the tray, present the maximum thickness. It can also be observed that the

thickness distribution is the narrowest in subsections 5 and 6 because they comprise the bottom edges of the tray where the material undergoes the greatest stretching. Peterson et al.[14] showed similar results; that is, a decrease in wall thickness in proportion to the distance down the mold. The rim almost preserves the original thickness of the sheet; however, it must be kept in mind that, as a general practice of film or sheet producers, the original thickness is usually greater than the nominal. For instance, a sheet with a nominal thickness of 450 μm can have a real thickness of between 450 and 475 μm.

Comparing the behavior of the two types of 3D corners, that is, the rounded corners corresponding to cross-section CS-2 (points P9, P10, P11, P12, P13) and the sharp corners corresponding to cross-section CS-3 (points P14, P15, P16, P17, P18, P19, P20), can provide useful insights. It can be observed that points 16 and 17 of the sharp corner underwent a greater thickness reduction than points P9 and P10, which are at the same depth of thermoforming but correspond to the round corner. This is due to the fact that, with the same quantity of material, sharp corners have a greater surface area, and the material is stretched to adapt to this wider surface.

The variability of the thickness is more relevant at points P7, P12, and P19 (Figure 3). These points correspond to subsections s_1 and s_2, located in the upper part of the walls of the tray, in the transition between the rim toward the bottom of the tray. During the thermoforming process, the thickness of a point is influenced by the contact time between the material and the cold walls of the mold. For instance, point P19 exhibits the greatest variability in most of the trays, because it is placed in the sharp corner close to the rim, and this leads to more variability because of the longer contact time between the mold and the material. It can also be observed that point P2, corresponding to CS-1 in s_8, at the bottom of the tray, is thicker when thermoforming at lower temperatures. This could be explained by the fact that at lower thermoforming temperatures, a milder stretching effect is produced on the bottom of the tray; in addition, the stretching effect is more marked on the walls than on the bottom. It must be taken into account that the measurements depend on the perpendicularity between the probe and the surface of the tray. Thus, at those points of the wall with an angle over the vertical (points P7, P12, and P19) the operator can introduce an error in the measurement if the probe is not vertical.

It must be highlighted that for each A-PET/PE material, the effect of the thermoforming temperature on thickness is negligible, as observed in Figure 3 for the tray with an initial thickness of 450 μm. Figure 4 shows the average thickness of each subsection for the same tray. The thickness distribution trend is the same for all the trays irrespective of the sheet thickness and the forming temperature. It can also be observed in Table 3 that, in subsection s_5, the thickness is almost the same for all the trays except for those of 600 μm and 650 μm, while in the remaining subsections, differences are detected in proportion to the initial thickness of the sheet.

3.2 | Oxygen permeation inside the tray: data and modeling

3.2.1 | Measured oxygen concentration

The evolution of the measured oxygen concentration versus time for the structure of 450 μm thermoformed at the

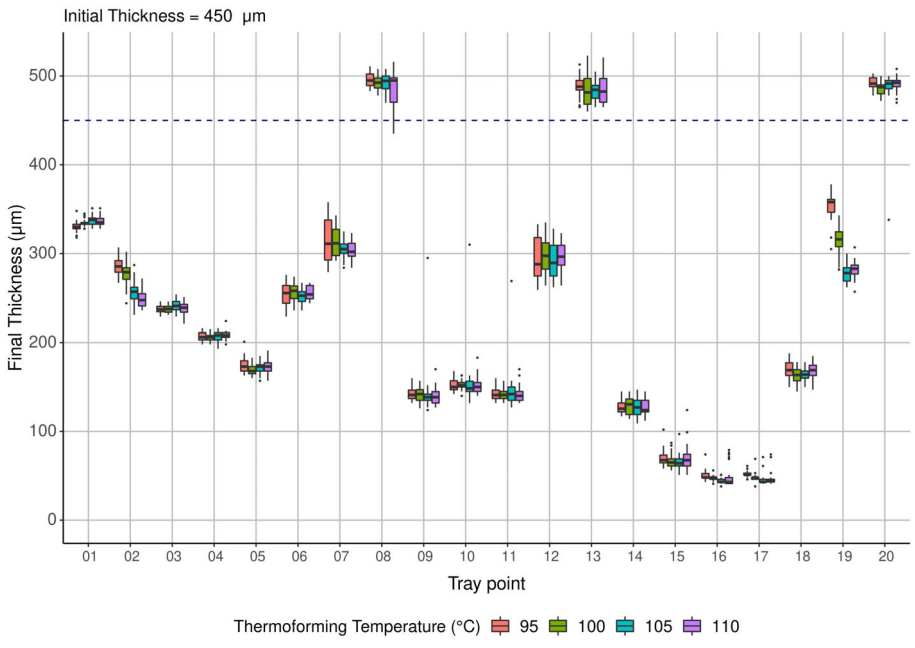

FIGURE 3 Average final thickness distribution of the PET/PE trays with an initial thickness of 450 μm

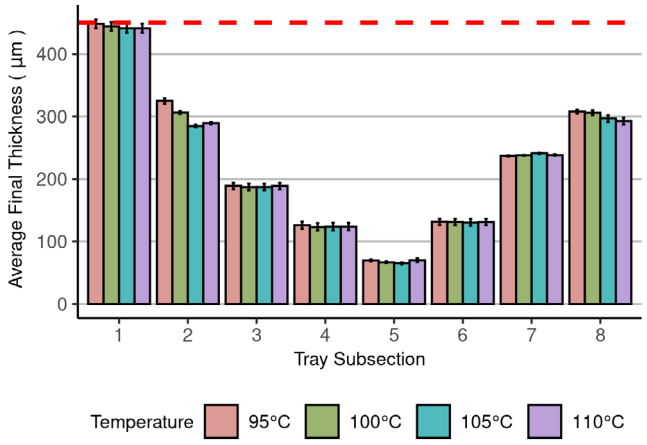

FIGURE 4 Average final thickness of each tray subsection after thermoforming for PET/PE trays with an initial thickness of 450 µm

predefined temperatures is shown in Figure 5, whereas the measured concentration corresponding to the average of the four thermoforming temperatures for each sheet is shown in Figure 6. The oxygen content inside the tray depends both on the residual oxygen after closing the lid and on the composition and initial thickness of the barrier layers, irrespective of the thermoforming temperature, since the temperature has been shown to have a mild influence on thickness distribution. Contrary to what was expected, no clear trend is observed between the initial thickness of the A-PET/PE sheets (450, 550, 600, 650 µm) and the oxygen permeation through the package walls, which disagrees with Kvalvag et al.[6] As for the A-PET/PE/EVOH/PE structure (750 µm), the EVOH increases the oxygen barrier of the tray, presenting substantial differences in the oxygen concentration against the A-PET/PE structures. These results are in accordance with the permeability data found in Buntinx et al.[5]

3.2.2 | Oxygen concentration modeling

When comparing the measured and calculated O_2 concentrations for A-PET/PE polymer combinations, the measured values are higher than the calculated ones (Figures 5 and 7). In the case of the structure with EVOH (A-PET/PE/EVOH/PE), the calculated and measured values are very similar (Figure 7). Pettersen et al.[14], who compared the measured and calculated OTR of thermoformed A-PET/PE and a polymer combination containing EVOH (PS/EVOH/PE), obtained similar results. However, other studies, such as that by Buntinx et al.[5] found that the measured OTR values of thermoformed A-PET/PE trays are a good approximation to the

TABLE 3 Surface area and thickness of each subsection into which the surface of the trays is divided

Subsection	Surface area (m^2)	Initial sheet thickness: 450 µm 95°C	100°C	105°C	110°C	550 µm 95°C	100°C	105°C	110°C	600 µm 95°C	100°C	105°C	110°C	650 µm 95°C	100°C	105°C	110°C	750 µm 105°C	110°C	115°C	120°C
s_1	$1.35{\cdot}10^{-2}$	389	386	386	387	462	469	469	471	498	508	509	510	541	544	550	553	642	642	640	659
s_2	$1.26{\cdot}10^{-2}$	279	275	269	272	337	334	330	329	360	364	358	361	398	398	393	384	423	459	449	453
s_3	$1.23\ 10^{-2}$	186	185	186	188	226	221	227	227	241	241	247	250	269	264	258	264	280	304	304	298
s_4	$0.57\ 10^{-2}$	127	127	130	130	160	151	158	158	174	168	172	175	190	182	176	184	209	207	210	206
s_5	$0.27\ 10^{-2}$	106	108	110	110	107	108	112	113	103	106	109	109	112	113	116	120	115	112	115	119
s_6	$0.77\ 10^{-2}$	117	117	121	120	147	141	146	147	163	156	159	161	170	165	164	171	199	189	192	190
s_7	$0.54\ 10^{-2}$	165	170	174	172	204	207	212	213	229	226	234	235	237	241	247	257	296	283	286	287
s_8	$2.59\ 10^{-2}$	206	208	208	206	261	264	259	257	294	290	286	281	313	316	319	312	383	360	364	355

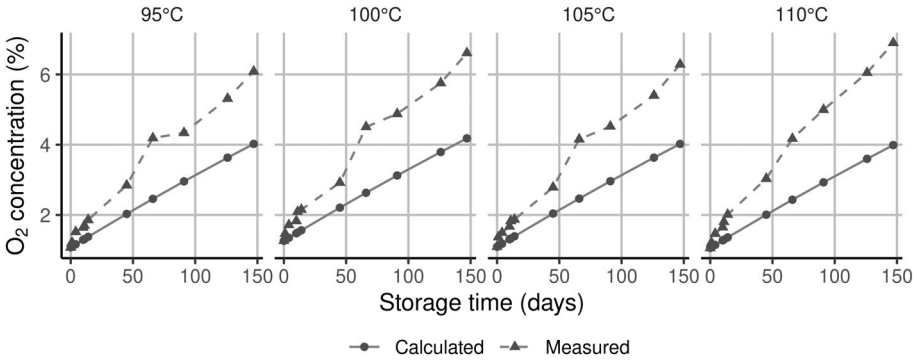

FIGURE 5 Evolution of the measured and calculated oxygen concentration versus time for the structure of 450 μm at each thermoforming temperature

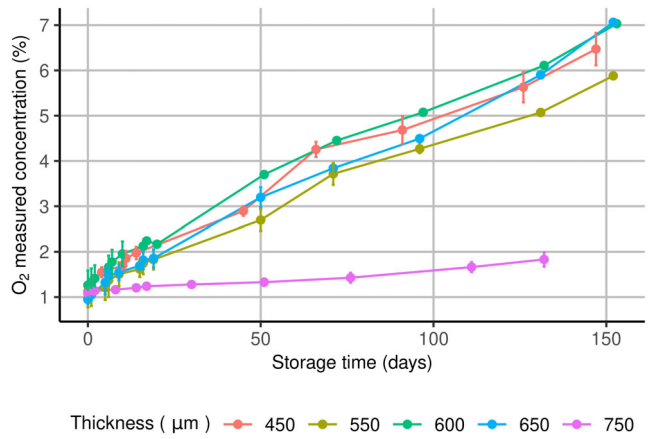

FIGURE 6 Measured oxygen concentration in the package headspace versus time for the thermoformed packages with different thicknesses. Each line represents the average concentration for all the thermoforming temperatures used for each thickness

calculated, except for the packages with the highest drawing depth, where the measured values are also higher than the calculated, these differences being greater for the thickest sheet. Those authors emphasized that oxygen permeates the amorphous sections of the material more easily than the crystallized. Thus, the lower the crystallinity degree of the polymer, the greater the permeability.[5] In fact, Lu and Hay[3] reported that orientation decreased as the temperature rose in the range between 75°C and 85°C, due to the relaxation of molecular chain segments. Based on this, Pettersen et al.[14] point out that other factors besides the area and thickness are influencing the OTR values, which are the two parameters taken into account to calculate the oxygen permeation in the present study. Hence, the high O_2 concentration measured in this study can be due to the fact that other process parameters, such as the thermoforming temperature or the drawing depth, were not optimally chosen for the A-PET/PE polymer combinations.

The assumption made in Equation (1) that OTRi is proportional to the area of the subsection ($A(s_i)$) and inversely related to the average thickness of the layer of the subsection (d_i) does not consider that during the thermoforming process, molecular changes can occur that significantly alter the permeability of the material. That is, depending on the heating process, the temperature distribution in the sheet, the stretching of each subsection of the tray, and the cooling process in the thermoforming mold, the permeability of the material could be different. The thermoforming process will thus affect the final properties of the packaging structure based on the material's intrinsic and inner features, such as chemical structure, crystallinity, glass transition temperature, and free volume.[20–23]

The calculated and measured O_2 concentration values have been plotted in Figure 7, while Table 4 gathers the regression results for each fit, including the lower and upper limits of the 95%-confidence interval both for the intercept and the slope as well as for the coefficient of determination. The measured and calculated values do not agree except for the 750 μm samples, which correspond to the structure with EVOH. However, for the rest of the thicknesses, a good linear correlation between the calculated and measured values, with R^2 coefficients of over 0.92, except for the 600 μm A-PET/PE trays.

For the A-PET/PE trays, the slope is always higher than 1 because the measured O_2 concentration values are higher than the calculated, as commented on above. In addition, as the A-PET/PE trays thicken, the slope of the line increases. This could be attributed to the relaxation effect of the molecular chains that try to recover the most energetically favorable state.[24] This relaxation is more marked for the greatest thickness. In fact, for these thicker sheets, when the heating time lengthens, the thermal inertia increases, favoring losses in molecule orientation, which in turn, could increase the crystallinity. Hence, the final permeability properties will depend on the contribution of both relaxation effect and crystallinity increase. Liu et al.[25] stated that the amorphous phase of PET dedensifies during crystallization, thereby increasing the permeability of the amorphous phase and reducing to some extent the other effects of orientation

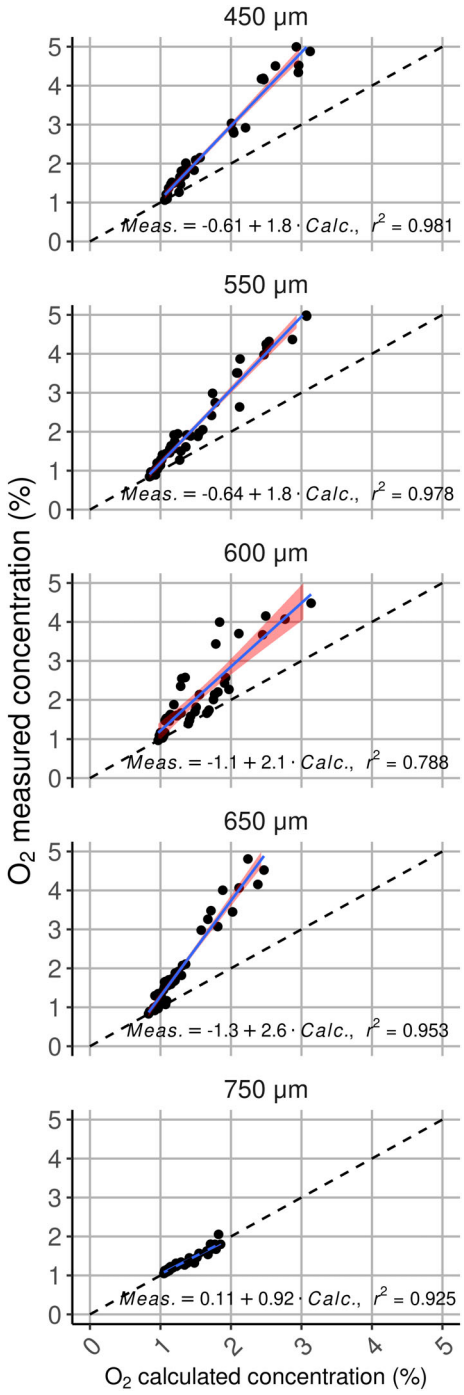

FIGURE 7 Calculated versus measured oxygen concentration in the package headspace for the different sheets at all the thermoforming temperatures

and crystallization. Amorphous phase dedensification is responsible for increased oxygen permeability despite the growth of impermeable crystals.[25] Hiltner et al.[26] came to the same conclusion, stating that the unexpected high gas permeability of crystalline PET is explained by the dedensification of the amorphous phase.

The regression analysis for the trays of 750 µm with an EVOH barrier (Figure 7) shows a good regression coefficient and a slope of nearly 1, since the predicted and observed values are very similar. This could mean that in sheets with EVOH, the thermoforming process does not seem to change the molecular orientation and crystallinity or that the changes do not affect the final permeability properties of the material. The barrier properties of EVOH are attributed to the inherent high degree of crystallinity and also to the size and distribution of the crystals. EVOH has a high crystallization rate as opposed to other thermoplastic polymers. Nevertheless, during thermoforming, the stretching of the polymer improves the orientation of the polymer chain originating lower oxygen permeability which compensates for the thickness reduction.[20] EVOH polymers can crystallize as the size of the hydroxyl groups is small relative to the space available in the crystal structure.[27] The changes in the crystallization of EVOH caused by the thermoforming process will depend on the strain rate, being lower when the strain is higher.[21]

The slope of the regression equations can be used to correct the simulated OTR for the A-PET/PE trays. In this way, the subsections contributing the most to the OTR of the tray can be detected. The contribution of one subsection to the OTR depends on the combined effects of both the surface area and the thickness. Thus, as can be observed in Figure 8, s_8 and s_6 are the subsections with the greatest contribution to OTR; s_8 because it is the subsection with the greatest surface area and s_6 due to its low thickness values (Table 3).

Different headspace volumes can be tested so as to estimate the influence of the headspace on the final oxygen concentration. A comparative test has been carried out with an empty tray of PET/PE/EVOH/PE 750 µm of 1800 cm^3 volume (Figure 8) and considering a food product that almost fills all the volume of the package, reducing the headspace to 10 cm^3 (Figure 9). As can be observed in Figure 9, this low headspace volume causes the rapid increase of the oxygen concentration inside the package.

The model also enables the evaluation of the potential deformation of the package by depressing or swelling effect, which is very important when it is necessary to guarantee both the integrity of the packages and a good presentation for consumers. With this aim, the model evaluates the global pressure inside the tray, adding all the partial pressures of the gases in the headspace (e.g., CO_2, N_2, and O_2). In Figure 10, it can be observed that for a tray with an initial 100% N_2 concentration, oxygen enters the package faster than nitrogen exits it, as oxygen presents a greater permeability than nitrogen. Consequently, over-pressure would happen at the

TABLE 4 Regression results using measured OTR as the criterion

Thickness (μm)	Predictor	*b*	*b* 95% CI [LL, UL]	*beta*	*beta* 95% CI [LL, UL]	sr^2	sr^2 95% CI [LL, UL]	*r*	Fit
450	(Intercept)	−0.61**	[−0.79, −0.43]						$R^2 = 0.981$**
450	Calculated	1.76**	[1.68, 1.83]	.99	[.95, 1.03]	0.98	[0.97, 0.99]	0.99**	95% CI [0.97, 0.99]
550	(Intercept)	−0.64**	[−0.79, −0.49]						$R_2 = 0.978$**
550	Calculated	1.84**	[1.76, 1.93]	.99	[.95, 1.03]	0.98	[0.96, 0.98]	0.99**	95% CI [0.96, 0.98]
600	(Intercept)	−1.06**	[−1.71, −0.41]						$R^2 = 0.788$**
600	Calculated	2.15**	[1.82, 2.48]	.89	[.75, 1.02]	0.79	[0.66, 0.85]	0.89**	95% CI [0.66, 0.85]
650	(Intercept)	−1.33**	[−1.62, −1.05]						$R^2 = 0.953$**
650	Calculated	2.59**	[2.42, 2.76]	.98	[.91, 1.04]	0.95	[0.92, 0.97]	0.98**	95% CI [0.92, 0.97]
750	(Intercept)	0.11*	[0.01, 0.22]						$R^2 = 0.925$**
750	Calculated	0.92**	[0.84, 1.00]	.96	[.88, 1.05]	0.93	[0.87, 0.95]	0.96**	95% CI [0.87, 0.95]

Note: A significant *b*-weight indicates that the beta-weight and semi-partial correlation are also significant. *b* represents unstandardized regression weights. *Beta* indicates the standardized regression weights. sr^2 represents the semi-partial correlation squared. *r* represents the zero-order correlation. LL and UL indicate the lower and upper limits of a confidence interval, respectively.* indicates $p < .05$. ** indicates $p < .01$.
Abbreviation: OTR, oxygen transmission rate.

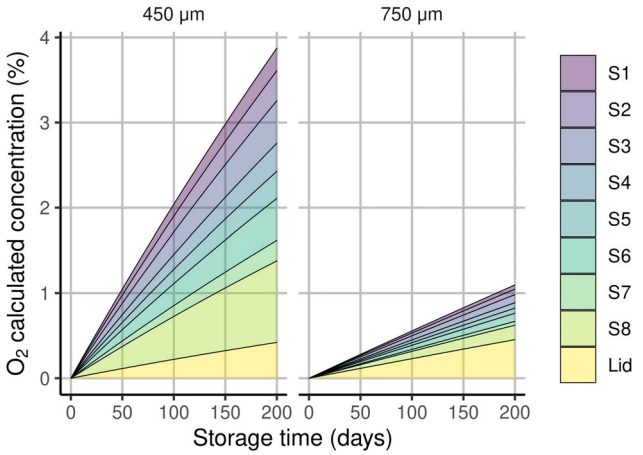

FIGURE 8 Contribution of each subsection to the calculated oxygen concentration in the package headspace versus storage time for PET/PE 450 μm and PET/PE/EVOH/PE 750 μm thermoformed at 110°C (headspace 1800 cm^3)

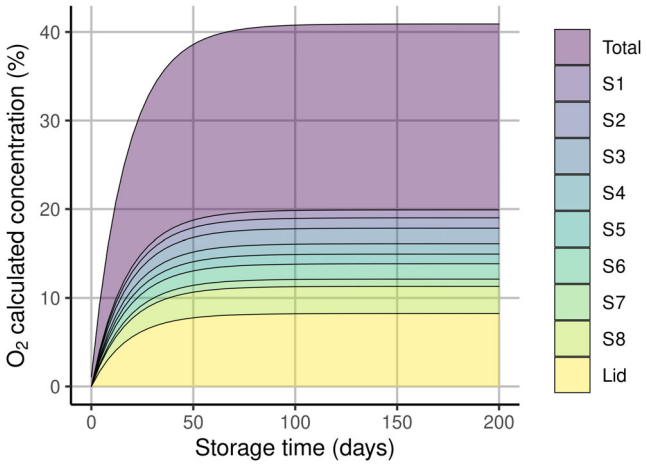

FIGURE 9 Contribution of each subsection to the oxygen concentration to the calculated oxygen concentration in the package headspace versus storage time for PET/PE/EVOH/PE 750 μm thermoformed at 110°C (headspace 10 cm^3)

beginning of the storage time, which would be asymptotically reduced over time.

It is common practice in the industry to use an estimated average thickness of a tray based on the initial thickness of the sheet in order to estimate the OTR of the thermoformed tray. The average thickness of a thermoformed tray is estimated considering that the volume of the sheet does not change after the thermoforming process and that the initial area of the sheet changes from 42,500 mm^2 to 85,600 mm^2 for the thermoformed tray. For instance, for a PET/PE tray with a thickness of 450 μm thermoformed at 110°C, an average thickness of 223.42 μm has been calculated. When comparing the oxygen concentration of trays simulated considering the measured thickness with that simulated using an average thickness, the oxygen concentration values are higher in the former. For instance, on day 200, the oxygen concentration reaches 4.93% with the measured thickness, 10% higher than the oxygen concentration estimated when considering the average thickness of the tray, which reaches 4.47%, which confirms the results of Kvalvag et al.[6]

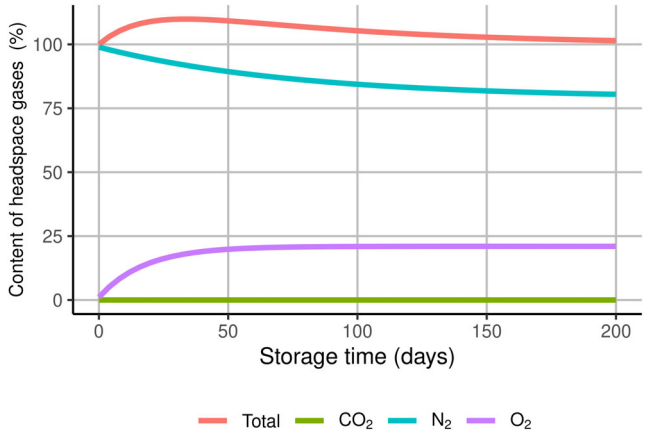

FIGURE 10 Calculated concentration of oxygen, nitrogen, and carbon dioxide content in the package headspace versus storage time for PET/PE/EVOH/PE tray of 750 μm thermoformed at 110°C (headspace 10 cm^3)

4 | CONCLUSIONS

The characteristics of a thermoformed packaging depend on variables, such as the initial sheet thickness, the depth and design of the mold, and the thermoforming parameters (temperature, heating time, pressing time, forming time, and pressure). In this study, the effect of the initial thickness and thermoforming temperature on the final thickness and OTR of the thermoformed trays' for two packaging materials (A-PET/PE and A-PET/PE/EVOH/PE) were studied. It has been observed that the range of the thermoforming temperatures does not affect the thickness distribution of the thermoformed trays, and nor, therefore, the OTR. 3D corners at the bottom of the tray undergo the greatest thickness reduction, decreasing by around 90%. The OTR of each tray has been measured experimentally and also estimated by considering the surface area and the average thickness of the different subsections of the thermoformed tray, which determine their contribution to the global OTR. However, the subsections affected by the thickness of these critical points have a small surface area, exhibiting a mild influence on the global OTR.

For A-PET/PE trays, the measured OTR is higher than that estimated with the model, while a good estimation was observed for the A-PET/PE/EVOH/PE trays. This means that other factors besides the area and thickness are influencing the OTR values of the A-PET/PE trays, these factors are more evident for the highest thickness values. From the reviewed literature, this can be attributed to changes in the polymer, such as the relaxation effect of the molecular chains of A-PET/PE, which affects the molecular orientation caused by the temperatures used in the thermoforming process, and also to the dedensification of the amorphous phase during the crystallization. In the case of the structure with EVOH polymer, the permeability of the material seems to remain unchanged, which according to the literature can be attributed to the orientation of the polymer chains during thermoforming. Thus, for the purposes of making an accurate estimation of OTR and depending on the polymer combination, studies are needed that evaluate the permeability changes brought about by the thermoforming process in order to correct the OTR estimation. In this way, the OTR model can be improved and can assist the selection of the sheet and the lid with compensated barrier properties to guarantee the shelf life of a packaged product. However, it should not be forgotten that designing proper packaging implies not only the selection of the material and the thickness of the sheets, but also other considerations beyond the scope of this article, such as mechanical properties and eco-design principles.

ACKNOWLEDGMENTS

The authors acknowledge the support from Klöckner Pentaplast (Spain), which provided the PET/PE sheets for the study, and Multivac Packaging Systems España S.L., which provided information on the thermoforming process for the machine.

DATA AVAILABILITY STATEMENT

Research data are not shared.

ORCID

Carlos Enguix https://orcid.org/0000-0002-6214-9957
Neus Sanjuan https://orcid.org/0000-0001-9413-0268
Javier Ribal https://orcid.org/0000-0002-9355-0145

REFERENCES

[1] P. V. Mahajan, F. A. R. Oliveira, J. C. Montanez, J. Frías, *Innov. Food Sci. Emerg.* **2007**, *8*, 84.
[2] M. Oksuz, C. Alsac, M. Ates, *Polym. Eng. Sci.* **2009**, *49*(11), 2234.
[3] X. F. Lu, J. N. Hay, *Polymer* **2001**, *42*(19), 8055.
[4] A. Makradi, S. Ahzi, S. Belouettar, D. Ruch, *Polym. Sci. Ser. A* **2008**, *50*, 550.
[5] M. Buntinx, G. Willems, G. Knockaert, D. Adons, J. Yperman, R. Carleer, R. Peeters, *Polymer* **2014**, *6*, 3019.
[6] M. Kvalvag, A. Nilsson, A. Espedal, A. Kohler, *Packag. Technol. Sci.* **2004**, *17*, 321.
[7] M. Jakobsen, L. Jespersen, D. Juncher, E. M. Becker, J. Risbo, *Packag. Technol. Sci.* **2005**, *18*, 265.
[8] R. Rodríguez-Aguilera, J. C. Oliveira, *Food Eng. Rev.* **2009**, *1*, 66.
[9] A. Abdellatief, B. A. Welt, *Packag. Technol. Sci.* **2012**, *26*, 281.
[10] S. Zekriardehani, S. A. Jabarin, D. R. Gidley, M. R. Coleman, *Macromolecules* **2017**, *50*, 2845.
[11] A. Aroujalian, M. O. Ngadi, J. P. Emond, *Polym. Eng. Sci.* **1997**, *37*, 178.

[12] J. Hertlein, R. P. Singh, H. Weisser, *J. Food Eng.* **1995**, *24*, 543.
[13] M. K. Pettersen, M. Gallstedt, T. Eie, *Packag. Technol. Sci.* **2004**, *17*(1), 43.
[14] M. K. Pettersen, A. Nilsson, A. Espedal, A. Kohler, *Packag. Technol. Sci.* **2004**, *17*(6), 321.
[15] F. Erchiqui, M. Souli, R. B. Yedder, *Polym. Eng. Sci.* **2007**, *47*(12), 2129.
[16] ASTM, *F1927 Standard Test Method for Determination of Oxygen Gas Transmission Rate, Permeability and Permeance at Controlled Relative Humidity through Barrier Materials Using a Coulometric Detector*, ASTM International, West Conshohocken, PA **2007**.
[17] I. Van Bree, B. De Meulenaer, S. Samapundo, A. Vermeulen, P. Ragaert, K. C. Maes, B. de Baets, F. Devlienghere, *Innov. Food Sci. Emerg.* **2010**, *11*(3), 511.
[18] M. Mastromatteo, M. A. Del Nobile, *J. Food Eng.* **2011**, *102*, 170.
[19] C. G. Soney, T. Sabu, *Prog. Polym. Sci.* **2001**, *26*, 985.
[20] C. Maes, W. Luyten, G. Herremans, R. Peters, R. Carleer, M. Buntinx, *Polym. Rev.* **2018**, *58*(2), 209.
[21] E. A. Franco-Urquiza, J. Gámez-Pérez, J. César, *Adv. Polym. Technol.* **2013**, *32*(S1), 287.
[22] C. Caner, *Packag. Technol. Sci.* **2011**, *24*, 259.
[23] S. Zekriardehani, A. S. Joshi, S. A. Jabarin, M. R. Coleman, *Polym. Cryst.* **2018**, *e10024*, 1.
[24] K. M. Hassan, M. Cakmak, *Macromolecules* **2015**, *48*, 4657.
[25] R. Y. F. Liu, Y. S. Hu, D. A. Schiraldi, A. Hiltner, E. Baer, *J. Appl. Polym. Sci.* **2004**, *94*, 671.
[26] A. Hiltner, R. Y. Liu, Y. Yushan, E. Baer, *J. Polym. Sci. Part B: Polym. Phys.* **2005**, *43*, 1047.
[27] K. Khanah, J. Tang, *Crit. Rev. Food Sci. Nutr.* **2012**, *52*(7), 640.

How to cite this article: C. Enguix, N. Sanjuan, J. Ribal, *Polym. Eng. Sci.* **2022**, *62*(11), 3599. https://doi.org/10.1002/pen.26130